

The shifting of secondary inorganic aerosols formation mechanism during haze aggravation: The decisive role of aerosol liquid water

Fei Xie^{1,2}, Yue Su^{1,3}, Yongli Tian², Yanju Shi², Xingjun Zhou², Peng Wang², Ruihong Yu¹, Wei Wang¹, Jiang He^{1,3}, Jinyuan Xin^{4,*}, Changwei Lü^{1,3,*}

¹ School of Ecology and Environment, Inner Mongolia University, 010021, Hohhot, China

² Inner Mongolia Environmental Monitoring Center, 010011, Hohhot, China

³ Institute of Environmental Geology, Inner Mongolia University, 010021, Hohhot, China

⁴ State Key Laboratory of Atmospheric Boundary Layer Physics and Atmospheric Chemistry (LAPC), Institute of Atmospheric Physics, Chinese Academy of Sciences, Beijing 100029, China

Abstract

Although many considerable efforts have been done to reveal the driving factors on haze aggravation, however, the roles of aerosol liquid water (ALW) in SIAs formation were mainly focused on the condition of aerosol liquid water content (ALWC) $<100\ \mu\text{g}/\text{m}^3$. Based on the in-situ high-resolution field observation, this work studied the decisive roles and the shifting of secondary inorganic aerosols formation mechanism during haze aggravation, revealing the different roles of ALWC in a broader scale ($\sim 500\ \mu\text{g}/\text{m}^3$) in nitrate and sulfate formation induced by aqueous chemistry in ammonia-rich atmosphere. The results showed that chemical domains of perturbation gas limiting the generation of secondary particulate matters presented obvious shifts from HNO_3 sensitive to HNO_3 and NH_3 co-sensitive regime with the haze aggravation, indicating the powerful driving effects of ammonia in ammonia-rich atmosphere. When $\text{ALWC}<75\ \mu\text{g}/\text{m}^3$, the sulfate generation was preferentially triggered by the high ammonia utilization, then accelerated by nitrogen oxide oxidation from Clean to Moderate pollution stages, characterizing as nitrogen oxidation ratio (NOR) <0.3 , sulfur oxidation ratio (SOR) <0.4 , ammonia transition ratio (NTR) <0.7 and the molar ratio of $\text{NO}_3^-/\text{SO}_4^{2-}=2:1$. While $\text{ALWC}>75\ \mu\text{g}/\text{m}^3$, aqueous-phase chemistry reaction of SO_2 and NH_3 in ALW became the prerequisite for SIAs formation driven by Henry's law in the ammonia-rich atmosphere during Heavy and Serious stages, characterizing as high SOR (0.5-0.9), NOR (0.3-0.5), NTR (>0.7) and the molar ratio of $\text{NO}_3^-/\text{SO}_4^{2-}=1:1$. A positive feedback of sulfate on nitrate production was also observed in this work due to the shift of ammonia partition induced by the ALWC variation during haze aggravation. It implies the target controlling of haze should not simply focus on SO_2 and NO_2 , more attention should be paid on gaseous precursors (e.g., SO_2 , NO_2 , NH_3) and aerosol chemical constitution during different haze stages.

Keywords: Mechanism shifting, Aerosol liquid water, Secondary inorganic aerosols, Haze aggravation, In-situ observation

* Corresponding author, Email: xjy@mail.iap.ac.cn; lcw2008@imu.edu.cn

1 Introduction

Fine particulate matter (PM_{2.5}) presented close link with several environmental issues, such as visibility reduction and climate change (Zhang et al., 2015; Shang et al., 2020; Wang et al., 2020; Wang et al., 2016; Nozière et al., 2010). Epidemiological studies have stated the association of PMs with various public health, even adverse birth outcomes (Gwynn et al., 2000; Lavigne et al., 2016; Zhao et al., 2020). As the most abundant secondary inorganic aerosols (SIAs) in PM_{2.5} during Chinese winter haze episodes (Fu and Chen, 2017; Liu et al., 2019), the formations of sulfate and nitrate play the key roles during haze aggravation, as well as the impacting factors of the oxidants in gas and aqueous phases, the characteristics of pre-existing aerosols/fog/cloud, and meteorological conditions. Recently, aerosol liquid water content (ALWC) was reported associating with the SIAs formation, especially sulfates and nitrates, during the haze periods (Wu et al., 2018; Zheng et al., 2015a; Wang et al., 2016; Cheng et al., 2016; Carlton and Turpin, 2013; Nguyen et al., 2014; Xue et al., 2014; Tan et al., 2017; Liu et al., 2017b). Atmospheric aerosol liquid water (ALW), which determined by ambient relative humidity (RH), has been proposed as a container since it could provide the reaction medium for the multiphase chemistry during the haze process (Ansari and Pandis, 2000; Shiraiwa et al., 2012; Davies and Wilson, 2015). The roles of ALWC on the generations of particulate sulfate generations (Wang et al., 2016; Cheng et al., 2016) and global secondary organic aerosols (Hodas et al., 2014; Mcneill, 2015; Wong et al., 2015) were reported. Thus, fully understanding ALW and its roles during haze aggravation is fundamentally important on atmospheric physicochemical processes, especially the liquid chemical transformation of SO₂ and NO_x in ALW.

Ammonia is the most important alkaline gas, neutralizing with acidic species to form ammonium salts. Due to little attention has been paid to NH₃ emissions by Chinese government, atmospheric NH₃ experienced a significant increasing trend (Ge et al., 2019; Tan et al., 2017). Although the increase in atmospheric NH₃ is beneficial to reduce atmospheric acidity (Liu et al., 2019), its chemical behavior on regional haze formation is still debating. Cheng et al. (2016) indicated that the fast transform of gaseous SO₂ to particle sulfate under polluted conditions is attributed to the neutralization of NH₃, which raises particle pH and thereby facilitated the aqueous oxidation of S (VI) by NO₂. Fang et al. (2017) stated that NH₃ partition significantly modified aerosol pH and thereby adjusting the partition of SO₂ and NO₂. Although the role of NH₃ has been identified from a theoretical perspective, the lack of NH₃ emission control sets barriers for more effective reduction of PM_{2.5}. Therefore, it is urgent to fully understand the reactive gases behavior and the chemical mechanism of SIAs formation during different

69 pollution stages, which will be helpful to propose reasonable strategies for each stage.

70 So far, the SIAs formation has been extensively studied during short-term, continuous, or
71 persistent haze episodes, proposing several heterogeneous and homogeneous oxidation
72 pathways on sulfate and nitrate formation (Guo et al., 2014; Guo et al., 2017; Zheng et al.,
73 2015b; Huang et al., 2014; Liu et al., 2021; Yao et al., 2020; Zhou et al., 2018; Liu et al., 2019).
74 In ammonia-rich atmosphere, NH₃ partition significantly modified aerosol pH, adjusted the
75 partition of SO₂ and NO₂ (Fang et al., 2017) and promotes the aqueous oxidation of S (VI) by
76 NO₂ (Wang et al., 2016; Cheng et al., 2016). Although many considerable efforts have been
77 done to reveal the driving factors on haze aggravation, however, the roles of ALW in SIAs
78 formation were mainly focused on the condition of ALWC < 100 μg/m³ (Nenes et al., 2020; Wu
79 et al., 2018; Bian et al., 2014; Jin et al., 2020). Therefore, the roles of ALWC in a broader scale
80 and the mechanism shifting of secondary inorganic aerosols formation during haze aggravation
81 in ammonia-rich atmosphere need to be understood in depth. Based on a continuous
82 observation with 1-hour resolution from December 2019 to January 2020, this work discussed
83 the shift of dominant mechanism with ALWC variation during the time window of haze
84 aggravation processes, which will be helpful to propose more effective PM_{2.5} control strategies
85 for each pollution stage.

86

87 **2 Sampling and Experiment Methods**

88 ***2.1 Description of Sampling Site***

89 Hohhot, the capital city of Inner Mongolia Autonomous Region, is the central city of Hohhot-
90 Baotou-Ordos group, as well as an important northern China city with a population of more
91 than 3.126 million and an area of 17224 km² (Fig. 1). This region is featured as continental
92 climate with marked seasonality changes, which characterized as long-lasting cold humid
93 winter and short-time other seasons. Thereby, to survive the cold season, approximately half
94 year of coal-fired heating events (Oct. 15-the following Apr. 15) were introduced, which
95 emitting gaseous pollutants as well as PMs around-the-clock. The main industries include
96 thermal power plants, coal-energy based biochemical industry, dairy industry and
97 petrochemical industry, etc., which also emit atmospheric pollutants ceaselessly. Thus, high
98 concentrations of PMs pollution cases dominated the major contamination cases during winter
99 season (data obtained from Department of Ecology and Environment of Inner Mongolia
100 Autonomous Region, <http://sthjt.nmg.gov.cn/>) and gradually emerging as the limiting factor on
101 regional ambient air quality and human health.

102 In this study, the observation was conducted at the Inner Mongolia Environmental

103 Monitoring Center (40°49'22"N, 111°45'2"E) on a top of a sixteen-story building (~40m above
104 the ground level) located at the eastern part of the downtown near the People's Government of
105 Inner Mongolia Autonomous Region near the 2nd ring road from December 1, 2019 to January
106 31, 2020. Residential and administrative regions were characterized as the major functional
107 domain near the sampling site, with no direct industrial regions nearby.

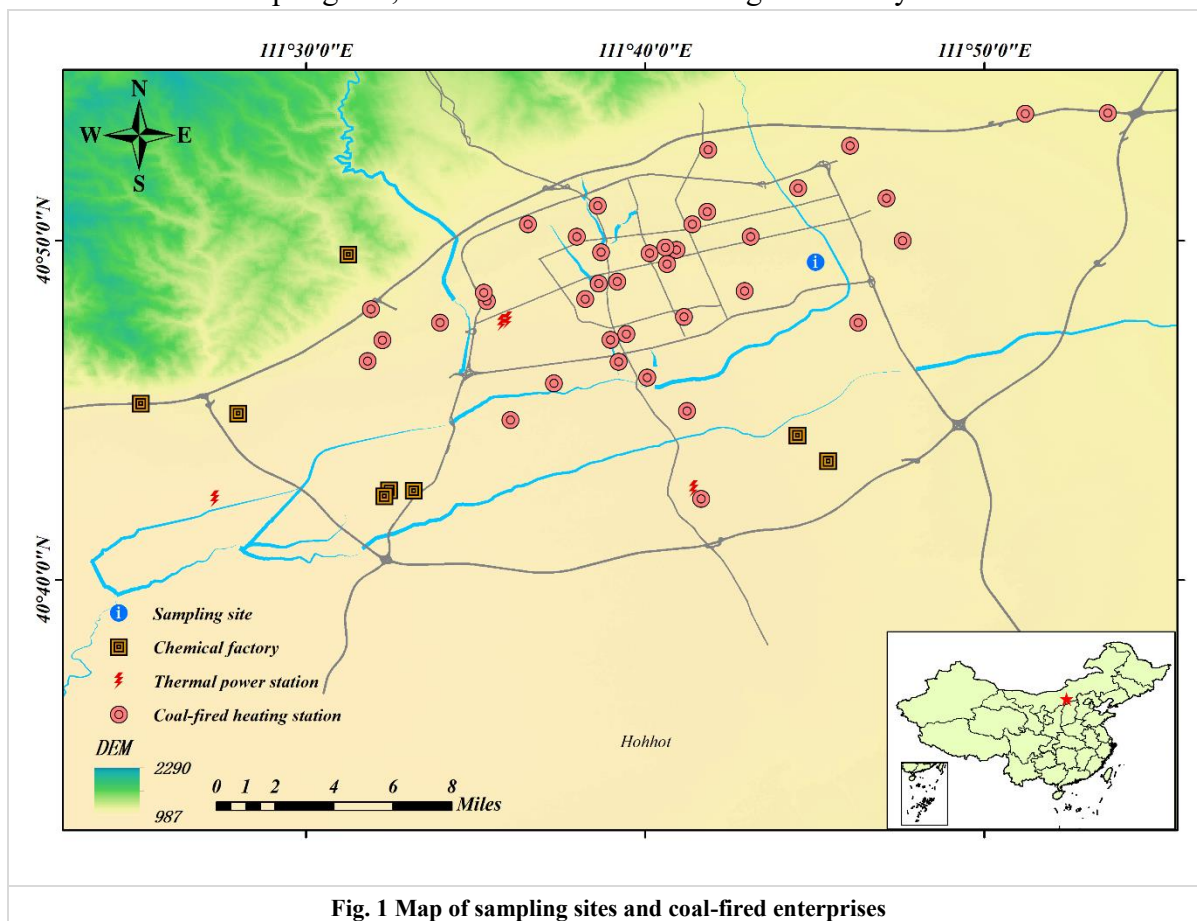


Fig. 1 Map of sampling sites and coal-fired enterprises

108

109 **2.2 Data acquisition and analysis methods**

110 **2.2.1 Data acquisition**

111 On-line ion-chromatograph instrument (MARGA ADI 2080, Metrohm Applikon, Switzerland)
112 was employed to simultaneously determine the water-soluble inorganic ions (Na^+ , NH_4^+ , Mg^{2+} ,
113 Ca^{2+} , K^+ , Cl^- , F^- , SO_4^{2-} , NO_3^-) in $\text{PM}_{2.5}$ and corresponding trace gases (SO_2 , HNO_2 , HNO_3 , HCl ,
114 NH_3). This instrument has been widely used in previous work (Rumsey et al., 2014; Nie et al.,
115 2015; Huang et al., 2020) and the details were listed in Supplement (S1.1). Correspondingly,
116 gaseous pollutants (e.g., NO_x , CO , PM_{10} , $\text{PM}_{2.5}$, PM_{10}) and meteorological datasets (e.g., wind
117 speed, wind direction, RH, temperature, etc.), as well as the adopted models could be found in
118 our previous work (Xie et al., 2021). In addition, peroxyacetyl nitrates (PANs), nitrous oxide
119 (N_2O) and solar spectrophotometry were measured by PANs-100 (Focused Photonics Inc.),

120 N₂O Monitor (LSE, Monitors) and CE-318T (CIMEL), respectively.

121

122 **2.2.2 Analysis methods**

123 Generally, sulfur oxidation ratio (SOR) and nitrogen oxidation ratio (NOR) were calculated as
124 follows, which were used to indicate the contribution of secondary transformation during the
125 haze events (Song et al., 2007; Zhou et al., 2018).

$$126 \quad SOR = \frac{n(SO_4^{2-})}{n(SO_2) + n(SO_4^{2-})}$$

$$127 \quad NOR = \frac{n(HNO_3) + n(NO_3^-)}{n(NO_2) + n(HNO_3) + n(NO_3^-)}$$

128 Meanwhile, as an indicator of ammonia conversion efficient, ammonia transition ratio
129 (NTR), was calculated as the following equation (All units were $\mu\text{g}/\text{m}^3$).

$$130 \quad NTR = \frac{NH_4^+/18}{NH_4^+/18 + NH_3/22.4}$$

131 In addition, as the fractions of ammonia, nitrate and sulfate in deliquesced aerosol, ε
132 (NO_3^-), $\varepsilon(\text{NH}_4^+)$ and $\varepsilon(\text{SO}_4^{2-})$ were expressed as follows.

$$133 \quad \varepsilon(\text{NO}_3^-) = \frac{n(\text{NO}_3^-)}{n(\text{HNO}_3) + n(\text{NO}_3^-)}$$

$$134 \quad \varepsilon(\text{NH}_4^+) = \frac{n(\text{NH}_4^+)}{n(\text{NH}_3) + n(\text{NH}_4^+)}$$

$$135 \quad \varepsilon(\text{SO}_4^{2-}) = \frac{n(\text{SO}_4^{2-})}{n(\text{SO}_2) + n(\text{SO}_4^{2-})}$$

136 **2.2.3 Aerosol pH**

137 In this work, a widely used thermodynamic model, ISORROPIA-II (Song et al., 2018; Gao et
138 al., 2020), was employed to establish aerosol acidity. Including the concentrations of WSIs in
139 $\text{PM}_{2.5}$ and gaseous pollutions (e.g., NH_3 , HCl), the simultaneously measured temperature and
140 RH data were imported into its Na^+ - K^+ - Ca^{2+} - Mg^{2+} - NH_4^+ - SO_4^{2-} - NO_3^- - Cl^- - H_2O aerosol system.
141 According to previous study (Song et al., 2018) and our data profiles, “Forward Mode” and
142 “Metastable State” were selected in the model of ISORROPIA-II to calculate aerosol acidity
143 (H_{air}^+ , H^+ loading per volume air ($\mu\text{g}/\text{m}^3$)) and aerosol liquid water content (ALWC). Then the
144 aerosol pH was calculated by the following equation.

$$145 \quad pH = -\log_{10} \frac{1000H_{\text{air}}^+}{ALWC}$$

146 The concentrations of NH_3 , NH_4^+ , NO_3^- and SO_4^{2-} modeled by this model significantly

147 correlated with their measured values with correlation coefficients of 0.971-0.999, indicating
 148 the accuracy and acceptability of the model in this work (Fig. S1).

149 **2.2.4 Heterogeneous sulfate production**

150 Due to the necessity of precise SO_4^{2-} generation, heterogeneous sulfate production (P_{het}) was
 151 parameterized and calculated according to the following equation (Jacob, 2000; Zheng et al.,
 152 2015a),

$$153 \quad P_{\text{het}} = \frac{3600sh^{-1} \times 96gmol^{-1} \times P \left(\frac{R_p}{D_g} + \frac{4}{v\gamma} \right)^{-1}}{R \times T} S_p[\text{SO}_2(g)]$$

154 Where P_{het} was presented in $\mu\text{g}\cdot\text{m}^{-3}\cdot\text{h}^{-1}$, $3600sh^{-1}$ is time conversion factor, 96 g/mol is the
 155 molar mass of SO_4^{2-} , P is atmospheric pressure in kPa, R is the gas constant with the value of
 156 $8.31 \text{ Pa}\cdot\text{m}^3\cdot\text{mol}^{-1}\cdot\text{K}^{-1}$, T is the temperature with the unit of K, R_p represented the radius of
 157 aerosol particles (m), D_g is the SO_2 molecular diffusion coefficient and v is the mean molecular
 158 speed of SO_2 with the typical tropospheric value of $2 \times 10^{-5} \text{ m}^2\cdot\text{s}^{-1}$ and $300 \text{ m}\cdot\text{s}^{-1}$, respectively. γ
 159 is the uptake coefficient of SO_2 on aerosols, S_p is the aerosol surface area per unit volume of
 160 air ($\text{m}^2\cdot\text{m}^{-3}$) (Jacob, 2000). $\text{PM}_{2.5}$ mass concentrations ($\mu\text{g}\cdot\text{m}^{-3}$) and mean radius (m) during
 161 campaign were roughly calculated utilizing the following empirical formula published by Guo
 162 et al. (2014):

$$163 \quad R_p = (0.254 \times C_{(\text{PM}_{2.5})} + 10.259) \times 10^{-9}$$

164 mean density of particles ρ was calculated and showed as $1.5 \times 10^6 \text{ g}\cdot\text{m}^{-3}$ using the volume
 165 and surface area formulas of a sphere (Guo et al., 2014). S_p was estimated from the following
 166 formula:

$$167 \quad S_p = \frac{C_{(\text{PM}_{2.5})} \times 10^{-6} \text{ g} \cdot \mu\text{g}^{-1}}{4/3 \cdot \pi R_p^3 \cdot \rho} \cdot 4\pi R_p^2$$

168 relative humidity-dependent γ were derived according to Zheng et al. (2015a) during the
 169 campaign in this work and showed as the following formular:

$$170 \quad \gamma = \begin{cases} 2 \times 10^{-5}, & \Psi \leq 50\%, \\ 2 \times 10^{-5} + \frac{5 \times 10^{-5} - 2 \times 10^{-5}}{100 - 50\%} \times (\Psi - 50\%), & 50\% \leq \Psi \leq 100\% \end{cases}$$

171 where ψ referred to RH with the unit of %.

172 **3 Results and Discussion**

173 Based on National Ambient Air Quality Standards of China (HJ633-2012)
 174 (https://www.mee.gov.cn/ywgz/fgbz/bz/bzwb/jcffbz/201203/t20120302_224166.shtml), air
 175 quality index (AQI) was introduced in this work to classify pollution levels (Wang et al., 2015;

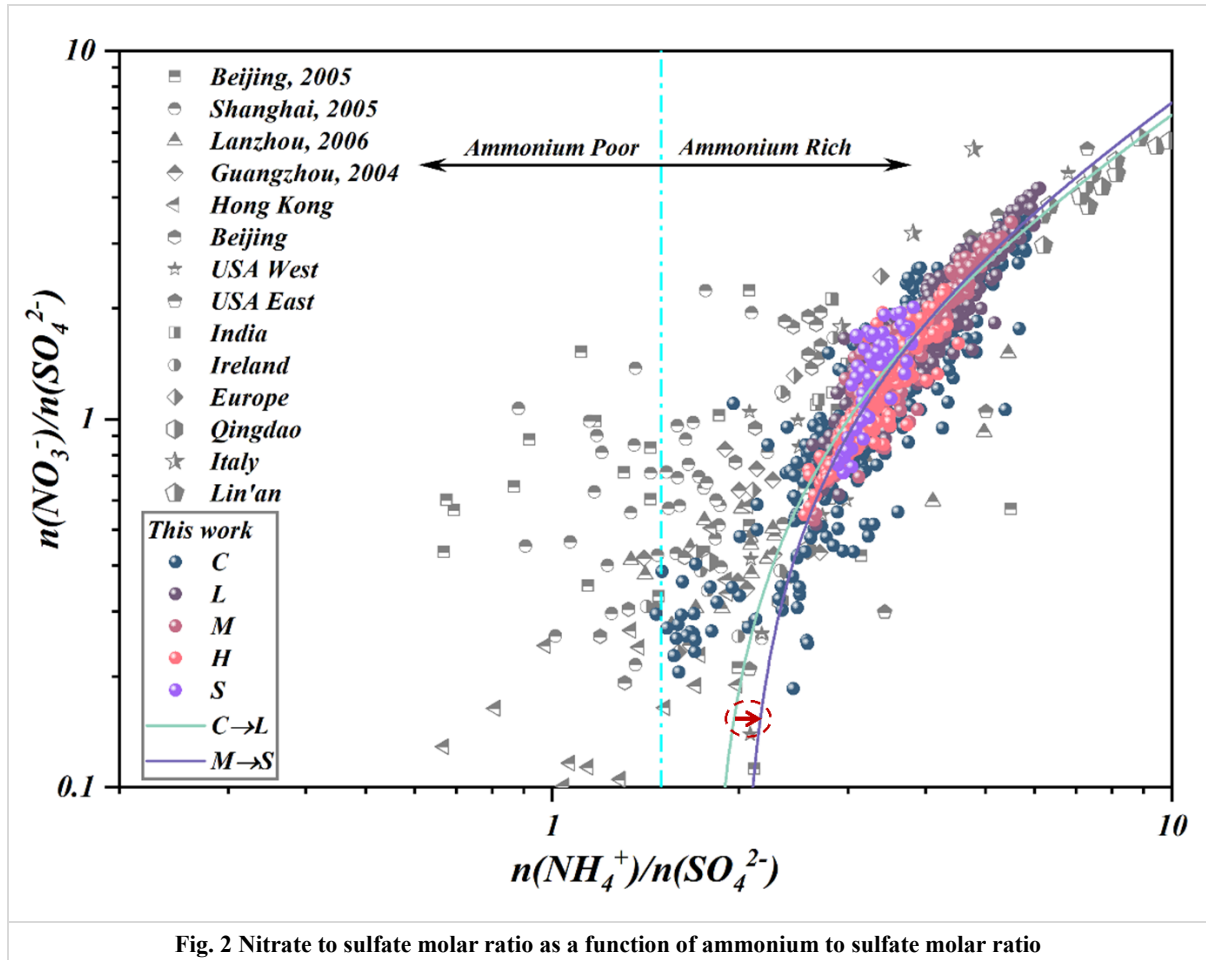
176 Kanchan et al., 2015; Xu et al., 2017) and discuss the characteristics of atmospheric pollutants.
177 Briefly, daily concentrations of PM_{2.5} ranged from 0-75, 75-115, 115-150, 150-250 and >250
178 $\mu\text{g}/\text{m}^3$ were classified as clean (C), light polluted (L), moderate polluted (M), heavy polluted
179 (H) and serious polluted (S) periods, respectively.

180 ***3.1 The observed evidence for ammonia-rich atmosphere***

181 The characteristics of atmospheric pollutants and meteorological parameters during the studied
182 period were summarized in Supplement (S2.1). In this work, molar ratios of NH_4^+ vs. anions
183 was used to identify the chemical species of ammonium salts (Zhou et al., 2018; Wang et al.,
184 2021; Liu et al., 2017b; Shi et al., 2019). The calculated results (Supplement, S2.2) showed the
185 predominant chemical species of ammonium gradually varied from the coexistence of
186 ammonium sulfate ($(\text{NH}_4)_2\text{SO}_4$) and ammonium nitrate (NH_4NO_3) to the coexistence of
187 $(\text{NH}_4)_2\text{SO}_4$, NH_4NO_3 and ammonium chloride (NH_4Cl) with haze aggravation (Fig. S5).
188 Further, the slope of fitted equation between excess- NH_4^+ and anions were still lower than 1:1
189 line after neutralized all the measured anions, indicating the ammonia-rich atmosphere (Fig.
190 S5c). To meet the national demand of ultra-low emissions activities (nearly two times lower
191 than former national standard) on gaseous pollutants, heavy usage of ammonia-containing
192 compounds in the process of desulfurization and denitrification (Solera García et al., 2017; Tan
193 et al., 2017) at broadly distributed thermal power plants (>300,000kWh) and the close-set coal-
194 fired heating stations (Fig. 1) resulted ammonia fugitive provided a reasonable explanation on
195 this ammonia-rich atmosphere. Although the retrofit of national demand of ultra-low emissions
196 activities on gaseous pollutants (nearly two times lower than former national standard) has
197 been completed, distributed coal-based enterprises could also emit substantial SO_2 and NO_2
198 and subjecting to heterogeneous reactions to further generate sulfate and nitrate and aggravated
199 the haze events (Fig. S7a, S7b).

200 To show the reaction between ammonia and nitric acid and the other formation processes
201 of nitrate in different (relative) concentrations of sulfate, the data of previous studies and
202 different pollution levels (C, L, M, H, S) in this work were plotted in Fig. 2. When
203 $[\text{NH}_4^+]/[\text{SO}_4^{2-}] \leq 1.5$, the nitrate formation associated with crustal elements rather than
204 ammonium; while $[\text{NH}_4^+]/[\text{SO}_4^{2-}] > 1.5$, the homogeneous gas-phase reactions between NH_3
205 and HNO_3 became the major pathway for atmospheric ammonia to form NH_4NO_3 (Pathak et
206 al., 2009; Liu et al., 2019). The results illustrated that the ammonia-rich regimes were not only
207 found in Hohhot, but also observed in Guangzhou (Huang et al., 2011), Chengdu (Huang et al.,
208 2018), Lanzhou USA West and East, India, Ireland, Europe, Qingdao, Italy, Lin'an (Pathak et
209 al., 2009) in recent decades (Fig. 2). It suggested that atmospheric oxidative modifications in

210 ammonia-rich atmosphere should be a widespread atmospheric issue with significant
 211 contributions on SIA generation. It was worth noting that the slopes of our data were becoming
 212 steeper, coupling with the $\text{NO}_3^-/\text{SO}_4^{2-}$ ratios change from ~ 4 to about 1, as the increasing
 213 pollution levels. The high $\text{PM}_{2.5}$ nitrate concentration during Heavy and Serious stages cannot
 214 be explained by the homogeneous gas-phase reaction involving ammonia and nitric acid, which
 215 may be associating with the heterogeneous reaction in ALW on the surface of the preexisting
 216 aerosols.



217

218 3.2 Driving mechanism of SIAs formation

219 3.2.1 Aerosol liquid water

220 Our results showed that SOR, NOR and SIAs in $\text{PM}_{2.5}$ presented increasing trends with the
 221 increasing ALWC during the five pollution levels. The variation of predominant chemical
 222 species of ammonium (Fig. 2) indicated more SIAs will be generated on particles with the
 223 simultaneous increase of ALWC and $\text{PM}_{2.5}$ (Fig.3b). Theoretically, the inorganic compounds
 224 conversion was enhanced via aqueous phase chemistry on moist particles owing to the
 225 continuous partition of gaseous pollutants (e.g., SO_2 , NO_2 , N_2O_5) in ALW, then disrupted the
 226 equilibrium between the gaseous and condensed phases, resulting in the aggravation of haze

227 events (Xue et al., 2014; Wu et al., 2018; Zheng et al., 2015b; Wang et al., 2016). Considering
228 seasonal heating characteristics, the shift of the equilibrium between gaseous and condensed
229 phases was enhanced with the increasing atmospheric pollutants concentrations due to the coal-
230 fired combustion events in winter. Detailly, owing to hygroscopic nature, the particles must
231 increase their water contents via ALW along with RH (Fig. S8a) to maintain thermodynamic
232 equilibrium and water vapor and simultaneously enhance the oxidation and dissolution of
233 precursors in the micro-solution (ALW) of the particulates. This process elevated the inorganic
234 mass fraction as well as particulate mass concentrations during different pollution stages (Fig.
235 S8b) (Bertram et al., 2009; Wang et al., 2016; Zheng et al., 2015a; Cheng et al., 2016). Due to
236 the larger affinity of H_2SO_4 for NH_3 (aq), sulfate was preferentially and fully neutralized by
237 ammonium in the ammonia-rich atmosphere to generate non-volatile nature of $(\text{NH}_4)_2\text{SO}_4$ (Liu
238 et al., 2017b; Zhou et al., 2018; Wang et al., 2021). Thus, SOR presented higher exponential
239 growth with the elevated AWLC coupling with more sulfate production (Fig. 3b).
240 Concomitantly, the preferentially generated $(\text{NH}_4)_2\text{SO}_4$ further enhanced the hygroscopicity of
241 particulate matter, in turn, helped more ammonia partitioning into moist particulate matter and
242 generating ammonium salts accelerating haze aggravation (Supplement, Fig. S6, Fig. S8c).
243 Thus, most important of all, the sharp increase of inorganic compounds associating with the
244 elevated ALWC significantly modified the specific surface area of particulates and further
245 accelerated the hygroscopic aerosol growth, which simultaneously provided a substrate for the
246 ensuing heterogenous reaction and accelerated the evolution of haze events. Previous work
247 reported that particles of different modes made different contributions to ALWC with the
248 contributions of nuclear, Aitken, accumulation and coarse modes assessed at <1%, 3%, 85%
249 and 12%, respectively, indicating that the contribution of accumulation mode particles to
250 ALWC dominated among all the aerosol particle modes (Tan et al., 2017). It indicated that
251 secondary aerosol formation mainly happens on these fine particles as the surface area and
252 volume of the fine particles are much larger than those of the coarse particles. Thus, the
253 observed significant correlations of ALWC with the ratios ($\text{PM}_{1.0}/\text{PM}_{2.5}$ and $\text{PM}_{2.5}/\text{PM}_{10}$) in
254 this work also indicated that the hygroscopic growth of fine particulate matter ($D_p \leq 2.5\mu\text{m}$)
255 strongly associated with ALWC (Fig. 3a). Both the previous work and our monitoring results
256 suggested that the ratios of $\text{PM}_{1.0}/\text{PM}_{2.5}$ and $\text{PM}_{2.5}/\text{PM}_{10}$ presented the potential possibility to
257 index the hygroscopic growth of particulate matter.

258

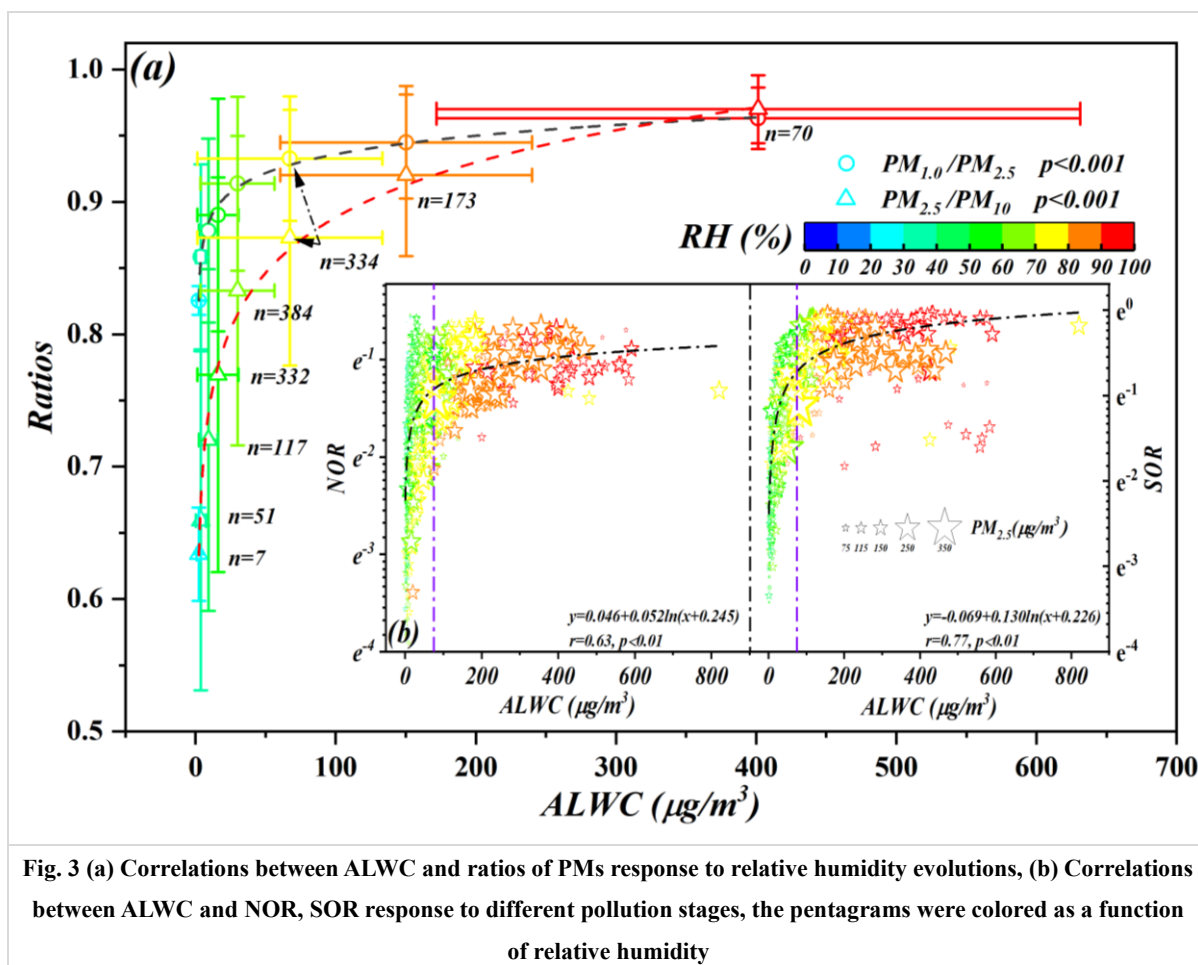


Fig. 3 (a) Correlations between ALWC and ratios of PMs response to relative humidity evolutions, (b) Correlations between ALWC and NOR, SOR response to different pollution stages, the pentagrams were colored as a function of relative humidity

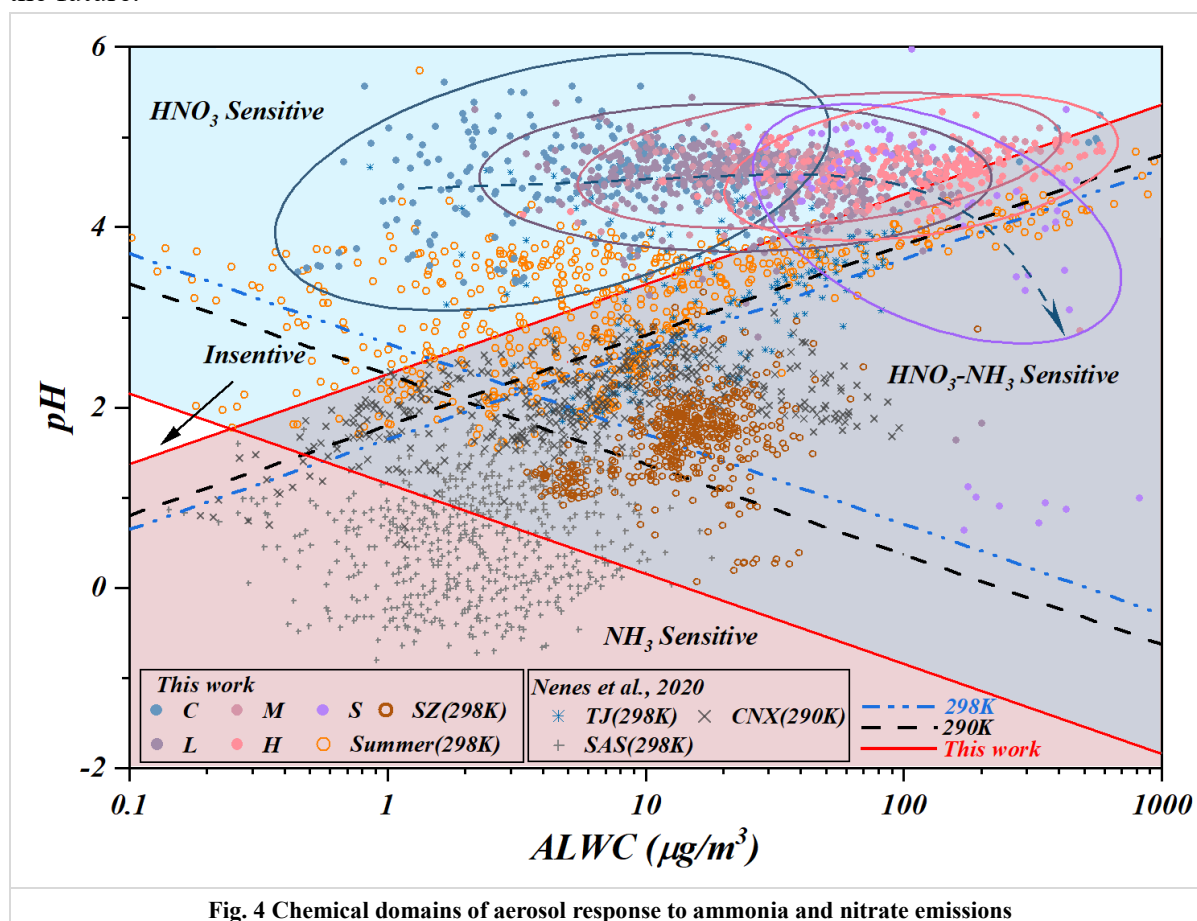
259 3.2.2 Perturbation gases

260 Due to the strict control of SO_2 , atmospheric concentrations of NO_2 and NH_3 gradually became
 261 as the decisive reactive precursors on regional atmospheric secondary particulate matter
 262 generation. Thus, the state-of-the-art framework proposed by Nenes et al. (2020) was carried
 263 out to exam the chemical domain classifications and the decisive precursor based on the data
 264 sets of previous studies (Nenes et al., 2020) and this work (Fig. 4). Due to the
 265 thermodynamically stable property of the preferentially generated $(\text{NH}_4)_2\text{SO}_4$, the semi-
 266 volatile NH_4NO_3 dominate the partitioning of NH_3^{T} (sum of NH_3 and NH_4^+ , same to NO_3^{T})
 267 and NO_3^{T} . Although aqueous NO_3^- concentrations varied with haze processes, the calculated ε
 268 (NO_3^{T}) (detailed calculated method could be found in S1.2), which was an equilibrium
 269 parameter between gaseous HNO_3 and particle-phase NO_3^- (Guo et al., 2016; Fang et al., 2017),
 270 presented consistently full loadings of nitrate on the existing particulates during the studied
 271 period (Fig. S9a, Fig. S9b). This could provide clear evidence for the initial HNO_3 sensitive
 272 area and continuous control of HNO_3 during the studied periods. However, with haze
 273 aggravation, significant elevated ALWC resulted in more precursors partitioned in micro-
 274 droplets to maintain water vapor. This process induced a positive shift of HNO_3 dissolution

275 equilibrium and leading more HNO₃ partitioned on particles driven by the Henry's law (e.g.,
 276 HNO_{3(g)}↔HNO_{3(aq)}, $K_H = 2.07 \text{ mol}/(\text{L}\cdot\text{Pa})$). Meanwhile, HNO₃ and HONO could also produce
 277 through the reactions of $\text{NO}_2 + \text{H}_2\text{O} \xrightarrow{\text{Het}} \text{HNO}_3 + \text{HONO}$ (Huang et al., 2018). Accordingly,
 278 the OH radicals generated by HONO photolysis also contributed to this oxidation processes
 279 (Yue et al., 2020; Zhu et al., 2020). These aqueous oxidations processes were evidenced by the
 280 observation of significantly elevated HONO and PANs during the haze aggravation
 281 (Supplement, Fig. S7c, Fig. S7d). Accordingly, the equations of $\text{NH}_4^+ + \text{NO}_3^- + \text{H}^+ + \text{OH}^- \rightleftharpoons$
 282 $\text{NH}_4\text{NO}_3 + \text{H}_2\text{O}$ and $\text{NH}_4^+ + \text{SO}_4^{2-} + \text{H}^+ + \text{OH}^- \rightarrow (\text{NH}_4)_2\text{SO}_4 + \text{H}_2\text{O}$ were shifted to
 283 generate more NH₄NO₃ and (NH₄)₂SO₄ (Nenes et al., 2020; Xie et al., 2020) due to the driving
 284 force of more ammonia partitioned in elevated ALWC ($\text{NH}_3 + \text{H}_2\text{O} \rightleftharpoons \text{NH}_3 \cdot \text{H}_2\text{O}$, $\text{NH}_3 \cdot \text{H}_2\text{O} \rightleftharpoons$
 285 $\text{NH}_4^+ + \text{OH}^-$). Therefore, NH₃ and NO_x became as the decisive factors on regional atmospheric
 286 oxidability in the ammonia-rich regime (Zhai et al., 2021; Tan et al., 2017; Liu et al., 2019; Li
 287 et al., 2019).

288 Generally, both NH₃ and HNO₃ were the limiting factors governing the aerosol generations
 289 for cities of North China due to high loadings of atmospheric ammonia, while NH₃ governed
 290 PM formation for the southeast US (SAS) (Zhao et al., 2020). Thanks to the raw data of
 291 Shenzhen (SZ) (Wang et al., 2022), we also calculated the ALWC and aerosol pH using
 292 ISORROPIA-II and the scatters of SZ suggested obvious chemical transition from HNO₃-NH₃
 293 regime to NH₃ sensitive regime due to the differently originated air masses. Although both
 294 cities located in US, the findings in California (CNX) were quite interesting and distributed in
 295 the insensitive region and the combined NH₃-HNO₃ sensitive region due to the moderate NH₃
 296 levels and the complicated atmospheric conditions during the observation (Nenes et al., 2020).
 297 In our work, the data points (541/744) in summer (pH=3.47±1.29) mostly lied in HNO₃
 298 sensitive region, while chemical domains of perturbation gas limiting the generation of
 299 secondary particulate matters presented obvious shifts from HNO₃ sensitive to HNO₃ and NH₃
 300 co-sensitive regime with the haze aggravation in winter. Some data points of this work lied in
 301 the combined NH₃-HNO₃ region in winter owing to the more acidic condition. Under the stable
 302 pH of aerosols in winter at Hohhot (pH=4-5), the more important is that a fraction of points
 303 will distribute in the combined NH₃-HNO₃ region when ALWC>75 μg/m³, which may be
 304 attributed to the aqueous chemical transformation driven by Henry's law mentioned above due
 305 to the elevating ALWC. Comparatively, the aerosols pH in summer was significantly lower
 306 than those in winter in Hohhot. Compared to TJ and SZ, the aerosols pH of Hohhot in winter
 307 was also significantly higher (Fig. 4) due to the acidity of atmospheric PM is largely depended
 308 on the alkaline material in surface soils in arid and semi-arid region and the elevated

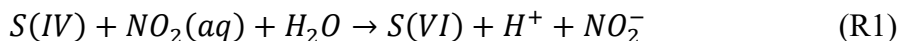
309 atmospheric ammonia. In terms of seasonal characteristics, the higher temperature in summer
 310 elevates the volatility of NH_4NO_3 and dominates the partitioning of NH_3^T in atmospheric phase
 311 to decrease the pH of aerosols. Therefore, as can be seen from Fig. 4, the data points measured
 312 in winter Hohhot characterized as higher pH and low ALWC than those in summer (Hohhot,
 313 SAS, CNX, SZ). According to the framework of Nenes et al. (2020), the transition points of
 314 Hohhot (whether winter or summer) between NH_3 -dominated and HNO_3 -dominated sensitivity
 315 also occurs at a pH around 2 but at lower levels of ALWC. Theoretically, it should be associated
 316 with the more aridity of Hohhot locating in the arid and semi-arid region of China. Our results
 317 provided the evidence for “the additional insight” proposed by Nenes et al. (2020) that the
 318 transition ALWC varies with season change and the aridity of sites, in response to seasonal
 319 variability and climate change. Although this effort could provide sound explanation for
 320 limiting gaseous pollutants on PM formation, mechanisms on their chemical domains,
 321 especially the roles of ALW in different locations with various conditions need further study in
 322 the future.



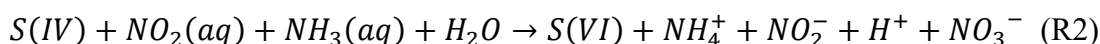
323 3.2.3 The shifting of SIAs formation mechanism driven by ALW

324 It's worth noting that two independent correlations were found between SOR and odd oxygen
 325 (O_x , $\text{O}_x = \text{NO}_2 + \text{O}_3$) during the aggravating processes of haze events, indicating the differential

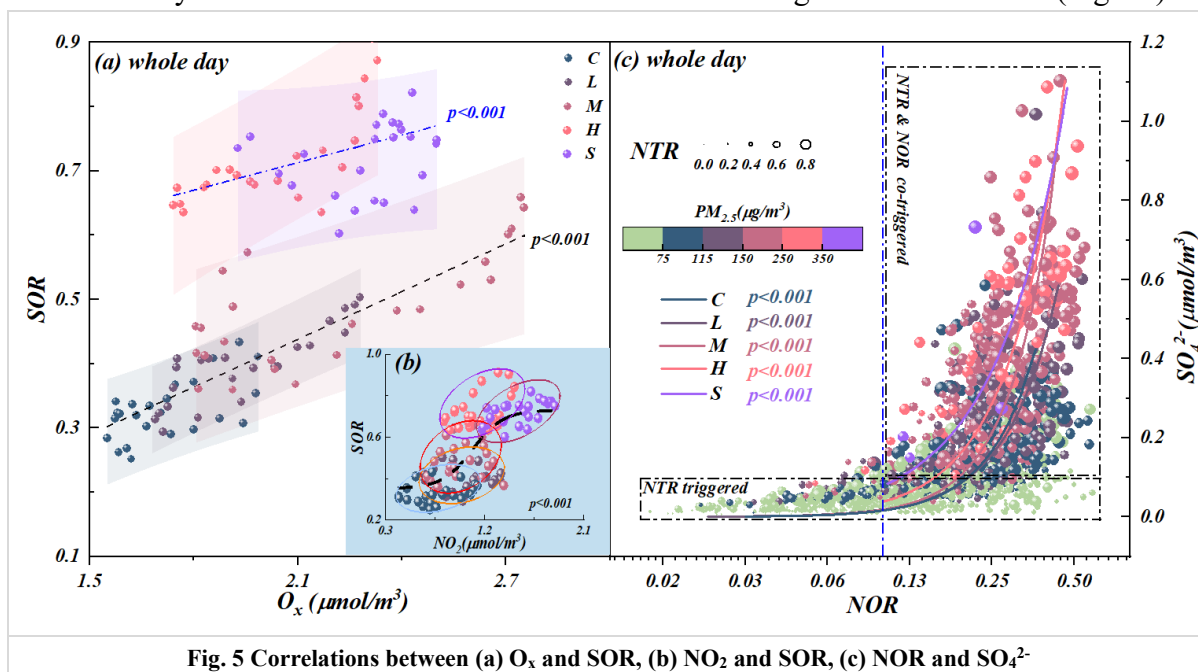
326 mechanisms of atmospheric oxidability on sulfate generations at different stages (Fig. 5a).
 327 Different to inefficient homogeneous sulfate oxidation efficiency (Supplement, Fig. S10),
 328 significant correlations pairs of NO_2 with SOR (Fig.5b) and NOR with SO_4^{2-} (Fig.5c) suggested
 329 the haze aggravation was largely related to the regional NO_2 levels due to the regulating effects
 330 on atmospheric oxidizability. Thus, the aqueous-phase oxidation of S(IV) by NO_2 (aq) was
 331 triggered and accelerated by the increasing ALWC and the following equation (Yao et al., 2020;
 332 Wang et al., 2016) (Supplement, Fig. S11a):



334 Meanwhile, sharp logarithmic increase between SOR and NH_4^+ were also observed from Clean
 335 to Moderate pollution stages (Supplement, Fig. S12). Due to the joint effects of ammonia-rich
 336 atmosphere and ammonia's extremely water-soluble property, sufficient hydroxide generated
 337 by ammonia dissolution forced the NO_2 partitioned in ALW to maintain pH through
 338 neutralization and producing sulfate via R1. Thus, the following equation (R2) was derived
 339 with considering the processes of ammonia hydrolysis, which was evidenced by Fig. S11b.



341 Generally, $\text{NOR} < 0.1$ means insignificant nitrogen oxide oxidation, therefore the observed
 342 regime shift of nitrate and ammonia chemical behavior on sulfate generation suggested the
 343 sulfate generation was preferentially triggered by the high ammonia utilization, then
 344 accelerated by the co-effects of ammonia utilization and nitrogen oxide oxidation (Fig. 5c).



345 Accordingly, the reaction R2 was activated due to the increased ALWC forced more
 346 ammonia to partition into moist particulate matter driven by the Henry's law in the ammonia-
 347 rich atmosphere ($\text{NH}_3(\text{g}) \rightarrow \text{NH}_3(\text{aq})$) (Supplement, Fig. S9c) (Clegg et al., 1998; Wu et al., 2018;

348 Xie et al., 2020). Meanwhile, our calculated aqueous generated NO_3^- nicely matched theoretical
349 nitrate aqueous generation curve (the solid blue line in Fig. S9b) proposed by Guo et al. (2017),
350 suggesting the pathway of fast sulfate formation from oxidation of S(IV) by NO_2 to generate
351 HONO (Wang et al., 2020) (Supplement, Fig. S11) via the reaction R2. As a result, the
352 thermodynamically stable $(\text{NH}_4)_2\text{SO}_4$ would be preferentially formed to maintain its water
353 vapor pressure and thermodynamic equilibrium, then triggered the haze formation. Thus, the
354 mentioned effects resulted in a pronounced increase of NH_3 partitioning with the haze
355 aggravation, suggesting the importance of ammonia partition on sulfate generations, namely,
356 NTR-controlled regime with $\text{ALWC} < 75 \mu\text{g}/\text{m}^3$. In summary, when $\text{ALWC} < 75 \mu\text{g}/\text{m}^3$, the
357 sulfate generation was preferentially triggered by high ammonia utilization, then accelerated
358 by nitrogen oxide oxidation from Clean to Light pollution stages (Fig. 5c) with $\text{NOR} < 0.3$,
359 $\text{SOR} < 0.4$ and $\text{NTR} < 0.7$. In this period, the chemical composition of SIAs characterized as the
360 molar ratio of $\text{NO}_3^-:\text{SO}_4^{2-}=2:1$ (Fig. 6).

361 When $\text{ALWC} > 75 \mu\text{g}/\text{m}^3$, the haze was aggravated from Moderate to Serious stages along
362 with the increasing ALWC. As a result of increase in ALW, large amount of H^+ was dissociated
363 during the generation of ammonium sulfate (Supplement, Fig. S13a). From Light to Moderate
364 pollution stages, the solubility SO_2 driven by Henry's law was self-limiting due to the acidity
365 effect in low ALWC (with $\text{ALWC} < 75 \mu\text{g}/\text{m}^3$). Therefore, low sulfate concentrations coupled
366 with low ALWC at the beginning of haze event (Supplement, Fig. S13a). However, due to the
367 co-effects of elevated ALWC and hygroscopic nature of pre-generated ammonia sulfate, H^+
368 concentrations were diluted and nearly constant in-situ pH with the increase of ALWC during
369 Heavy and Serious pollution stages (Supplement, Fig. S14) (Wang et al., 2016; Clifton et al.,
370 1988; Huie and Neta, 1986; Lee and Schwartz, 1982). Hence, the significantly elevated ALWC
371 provided more chance for the partition of SO_2 , NO_2 and NH_3 in ALW from Moderate to Serious
372 pollution stages. Theoretically, Henry's constants of NO_2 ($9.74 \times 10^{-8} \text{ mol} \cdot (\text{L} \cdot \text{Pa})^{-1}$) is 3-4 orders
373 of magnitude lower than those of SO_2 ($1.22 \times 10^{-5} \text{ mol} \cdot (\text{L} \cdot \text{Pa})^{-1}$) and NH_3 (6.12×10^{-4}
374 $\text{ mol} \cdot (\text{L} \cdot \text{Pa})^{-1}$), however, it is worth noting that the aqueous generated NO_3^- from Moderate to
375 Serious stages rapidly increased 2-5 times higher than Clean and Light stages (Supplement,
376 Fig. S9b). Meanwhile, according to our monitoring results, the solar spectrophotometry at
377 380nm during Moderate to Serious stages was significantly lower than that in Clean stage
378 (Supplement, Fig. S15), suggesting the aqueous oxidation of NO_2 was the predominant
379 compared to chain photolysis (Huang et al., 2018). Accordingly, it could be deduced that
380 aqueous-phase chemistry reaction of SO_2 and NH_3 in ALW, driven by Henry law, became the
381 dominant mechanism for sulfate formation due to more NO_2 was required to take part in the

382 fast sulfate formation with the increase of ALWC in the ammonia-rich atmosphere by the
 383 reaction R2. Thus, with the increasing of ALWC, high concentrations of sulfate and nitrate with
 384 high SOR (0.5-0.9), NOR (0.3-0.5) and NTR (>0.7) induced the haze events becoming Heavy
 385 and Serious levels (Fig. 5c). Simultaneously, the calculated heterogeneous sulfate production
 386 rate (Jacob, 2000; McNeill, 2015) (Supplement, Fig. S16) presented similar trends with the
 387 impacts of ammonia on sulfate production during different pollution stages (Xue et al., 2016;
 388 Cheng et al., 2016; Liu et al., 2020). It further stated the environmental significance of the
 389 partitioning of SO₂ and NH₃ between gas and aqueous (ALW) phases for SIAs formation and
 390 haze aggravation. Our results provided the evidence of significant negative correlations
 391 between HONO and N₂O (Supplement, Fig. S17) from Moderate to Serious stages and positive
 392 correlations between HONO and SOR (Supplement, Fig.S11a), highlighting the recent reported
 393 secondary aqueous-phase oxidation pathway of SO₂ by HONO from moderate pollution period
 394 ($2N(III) + 2S(IV) \rightarrow N_2O \uparrow + 2S(VI) + other\ products$) (Wang et al., 2020). In summary,
 395 when ALWC > 75 μg/m³, aqueous-phase chemistry reaction of SO₂ and NH₃ in ALW became
 396 the prerequisite for SIAs formation driven by Henry's law in the ammonia-rich atmosphere
 397 during Heavy and Serious stages with high SOR (0.5-0.9), NOR (0.3-0.5), NTR (>0.7). In this
 398 period, the chemical composition of SIAs characterized as the molar ratio of NO₃⁻:SO₄²⁻=1:1
 399 (Fig. 6).

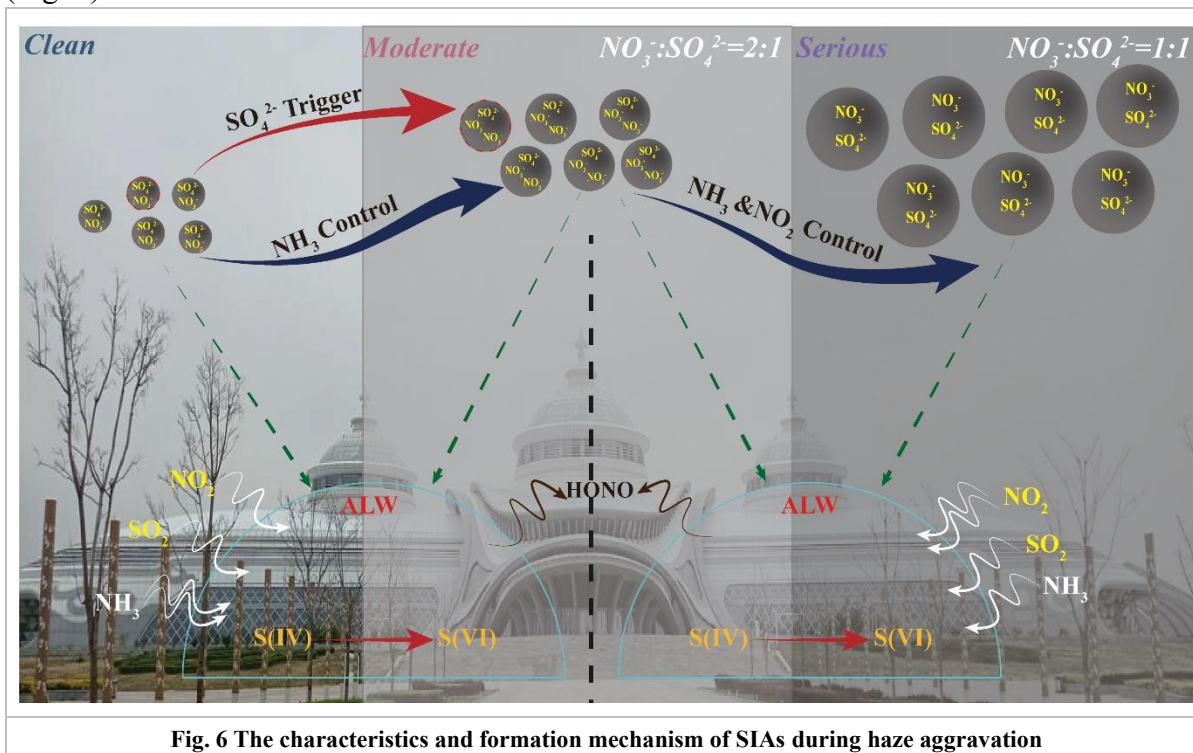
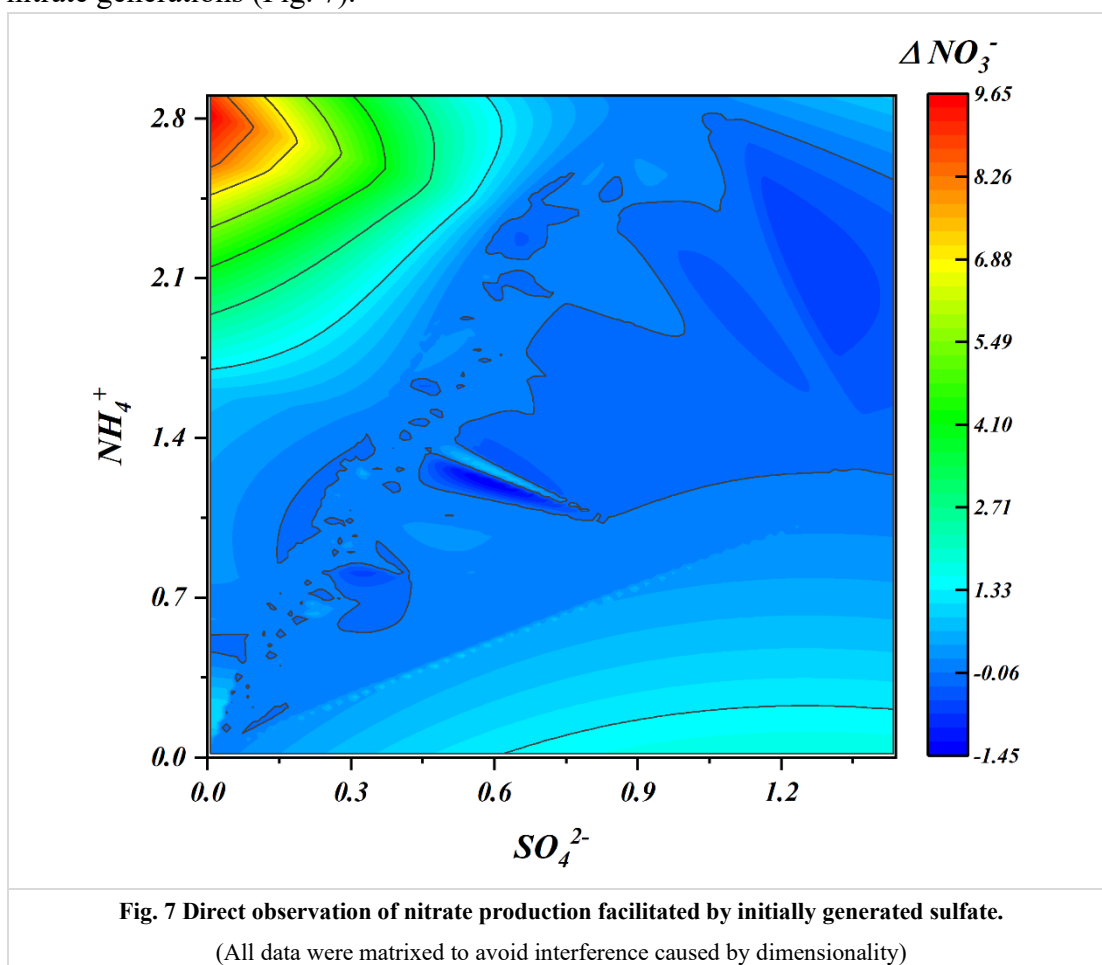


Fig. 6 The characteristics and formation mechanism of SIAs during haze aggravation

400

401 **3.2.4 The positive feedback of sulfate on nitrate production**

402 Previous works suggested that the homogeneous reaction of NO_2 with OH radicals during
403 daylight and heterogeneous hydrolysis of N_2O_5 at night were the main routes on nitrate
404 formation during haze episodes (He et al., 2018; Liu et al., 2020; Liu et al., 2019). Unsurprising,
405 higher nitrate production rates (ΔNO_3^- , the difference of hour concentrations and matrixing
406 afterwards) were frequently observed in ammonia-rich conditions due to that ammonia-rich
407 regime was more conducive on nitrate generation. However, the high level of nitrate production
408 rates (ΔNO_3^-) were found in the area characterizing as high ammonium and low sulfate levels,
409 suggesting that highly utilizing ammonium and pre-generated sulfate promoting particle-phase
410 nitrate generations (Fig. 7).



411

412 Here, we proposed a hypothesis about the hydrogen ion concentration to respond the
413 above observations. As is known to all, apart from the extremely low levels of crustal elements,
414 ammonia is the only alkaline gas to neutralize the acidic gases in the atmosphere and generate
415 ammonium ions (Xie et al., 2020). Thus, the concentrations of particulate sulfate and nitrate
416 are affected by the partitioning of $\text{NH}_4^+/\text{NH}_3$. Thereby, higher values of ΔNO_3^- and ΔSO_4^{2-}

417 always occurred in the regions with higher ammonium ions were not confused (Fig. 7, Fig.
418 S18). According to both our results and published laboratory work (Wang et al., 2016), the
419 acidity of the particulate matter could be significantly modified by the bulk aqueous reaction
420 between NO_2 and SO_2 , in which this reaction could be further enhanced due to in the presence
421 of NH_3 . As a result of the increase in RH, the partitioning of atmospheric ammonia was broken
422 in a deep extent, which enhanced the neutralization of S(VI) by ammonia at the particle surface
423 to generate ammonium sulfate and dissociate huge H^+ (Fig. S13b, red part). Simultaneously,
424 the ALWC did not raised significantly (Fig. S14b) at the beginning of haze event with relative
425 low sulfate concentrations. Thus, hydrogen ions generated from sulfate dissociation absorb
426 ammonia more effectively from the ammonia-rich atmosphere at low relative humidity during
427 the early pollution stages, which significantly promotes the net nitrate production. However,
428 due to the co-effects of elevated RH and hygroscopic nature of pre-generated ammonia sulfate,
429 H^+ concentrations were diluted and shown as nearly constant in-situ pH (Fig. S14a). According
430 to previous works, the reaction between firstly generated sulfate and bisulfate with ammonia
431 were treated as the determination reaction on particle acidity (Weber et al., 2016; Liu et al.,
432 2017a). This reaction is self-limiting due to the acidity effect, namely that it increases the
433 acidity of aqueous phase and in turn reduces the efficiency of Henry's constant for SO_2
434 solubility and reaction rate and reduced the H^+ formation rates from moderate periods,
435 compared with clean periods (Fig. S13b, blue) (Wang et al., 2016; Clifton et al., 1988; Huie
436 and Neta, 1986; Lee and Schwartz, 1982). Due to the co-effects of RH increase and
437 hygroscopic of sulfate, the ALWC was significantly elevated with the worsen of haze. Although
438 more H^+ was generated in this process, no significant decrease in pH was found with the haze
439 aggravation due to the dilution effect of ALWC on H^+ . Previous works suggested that in the
440 case of ALWC increase, nitrate production is controlled by elevated H^+ associating with the
441 increase of sulfate, namely, NO_3^- presented elevating trend with the increases of H^+
442 concentration (Xie et al., 2020). Thus, although H^+ from the dissociation of sulfuric acid and
443 full-loaded particle nitrate in conjunction with the haze aggravation generate particle HNO_3
444 (Fig. S19a) could forcing more ammonia partitioned on the particles to generate ammonium
445 nitrate (Fig. S19b), net nitrate production (ΔNO_3^-) was nearly consistent.

446 **4 Conclusions**

447 The formation of SIAs, especially sulfates and nitrates, was inherently associated with ALWC
448 during the haze aggravation, in which the roles of ALWC should be more significant in
449 ammonia-rich atmosphere. The novelty of our work is to find the shifting of secondary
450 inorganic aerosols formation mechanism during haze aggravation and explain the different

451 roles of ALWC in a broader scale ($\sim 500 \text{ ug/m}^3$) in ammonia-rich atmosphere based on the in-
452 situ high-resolution on-line monitoring data sets. The results showed that chemical domains of
453 perturbation gas limiting the generation of secondary particulate matters presented obvious
454 shifts from HNO_3 sensitive to HNO_3 and NH_3 co-sensitive regime with the haze aggravation,
455 indicating the powerful driving effects of ammonia in ammonia-rich atmosphere. When
456 $\text{ALWC} < 75 \text{ ug/m}^3$, the sulfate generation was preferentially triggered by the high ammonia
457 utilization, then accelerated by nitrogen oxide oxidation from Clean to Moderate pollution
458 stages, characterizing as $\text{NOR} < 0.3$, $\text{SOR} < 0.4$, $\text{NTR} < 0.7$ and the molar ratio of $\text{NO}_3^- : \text{SO}_4^{2-} = 2:1$.
459 While $\text{ALWC} > 75 \text{ ug/m}^3$, aqueous-phase chemistry reaction of SO_2 and NH_3 in ALW became
460 the prerequisite for SIAs formation driven by Henry's law in the ammonia-rich atmosphere
461 during Heavy and Serious stages, characterizing as high SOR (0.5-0.9), NOR (0.3-0.5), NTR
462 (> 0.7) and the molar ratio of $\text{NO}_3^- : \text{SO}_4^{2-} = 1:1$. A positive feedback of sulfate on nitrate
463 production was also observed in this work. Our work provides a potential explanation for the
464 interactive mechanism and feedback between nitric aqueous chemistry and sulfate formation
465 in ammonia-rich atmosphere based on high-resolution field observation. It implies the target
466 controlling of haze should not simply focus on SO_2 and NO_2 , more attention should be paid on
467 gaseous precursors (e.g., SO_2 , NO_2 , NH_3) and aerosol chemical constitution during different
468 haze stages.

469

470 *Data availability.* All data of this study are available from the corresponding author upon
471 reasonable request (lcw2008@imu.edu.cn).

472

473 *Supplement.* The Supplement related to this article is available online at

474

475 *Author Contributions.* FX: Data curation, Formal analysis, Software, Writing-original draft.
476 YS: Investigation, Formal analysis. YLT: Methodology, Software. YSH: Investigation, Formal
477 analysis. XJZ: Investigation, Formal analysis, Software. PW: Methodology, Investigation.
478 RHY: Software, Writing-review & editing. WW: Investigation, Validation, Writing-review &
479 editing. JH: Investigation, Methodology. JYX: Investigation, Validation, Supervision, Writing-
480 review & editing. CWL: Initiating and leading this research, Supervision, Writing-review &
481 editing.

482

483 *Competing interest.* The authors declared that they have no conflict of interest.

484

485 *Acknowledgments.* This work is supported by Science and Technology Major Project on Air
486 Pollution Prevention and Prediction in Hohhot-Baotou-Ordos Cities Group of Inner Mongolia
487 (No. 2020ZD0013), National Natural Science Foundation of China (No. 42167028, 41763014)
488 and Science Fund for Distinguished Young Scholars of Inner Mongolia (2019JQ05).
489

490 **References**

- 491 Ansari, A. S. and Pandis, S. N.: Water Absorption by Secondary Organic Aerosol and Its Effect on Inorganic
492 Aerosol Behavior, *Environ. Sci. Technol.*, 34, 71-77, 10.1021/es990717q, 2000.
- 493 Bertram, T. H., Thornton, J. A., Riedel, T. P., Middlebrook, A. M., Bahreini, R., Bates, T. S., Quinn, P. K., and
494 Coffman, D. J.: Direct observations of N₂O₅ reactivity on ambient aerosol particles, *Geophys. Res. Lett.*, 36,
495 <https://doi.org/10.1029/2009GL040248>, 2009.
- 496 Bian, Y. X., Zhao, C. S., Ma, N., Chen, J., and Xu, W. Y.: A study of aerosol liquid water content based on
497 hygroscopicity measurements at high relative humidity in the North China Plain Atmos. Chem. Phys., 14,
498 6417–6426, <https://doi.org/10.5194/acp-14-6417-2014>, 2014.
- 499 Carlton, A. and Turpin, B.: Particle partitioning potential of organic compounds is highest in the Eastern US and
500 driven by anthropogenic water, *Atmos. Chem. Phys.*, 13, 10203-10214, 2013.
- 501 Cheng, Y., Zheng, G., Wei, C., Mu, Q., Zheng, B., Wang, Z., Gao, M., Zhang, Q., He, K., Carmichael, G., Pöschl,
502 U., and Su, H.: Reactive nitrogen chemistry in aerosol water as a source of sulfate during haze events in
503 China, *Sci. Adv.*, 2, e1601530, 10.1126/sciadv.1601530, 2016.
- 504 Clegg, S. L., Brimblecombe, P., and Wexler, A. S.: Thermodynamic Model of the System H⁺-NH₄⁺-SO₄²⁻-NO₃⁻
505 -H₂O at Tropospheric Temperatures, *J. Phys. Chem. A*, 102, 2137-2154, 10.1021/jp973042r, 1998.
- 506 Clifton, C. L., Altstein, N., and Huie, R. E.: Rate constant for the reaction of nitrogen dioxide with sulfur(IV) over
507 the pH range 5.3-13, *Environ. Sci. Technol.*, 22, 586-589, 10.1021/es00170a018, 1988.
- 508 Davies, J. F. and Wilson, K. R.: Nanoscale interfacial gradients formed by the reactive uptake of OH radicals onto
509 viscous aerosol surfaces, *Chem. Sci.*, 6, 7020-7027, 10.1039/C5SC02326B, 2015.
- 510 Fang, T., Guo, H., Zeng, L., Verma, V., Nenes, A., and Weber, R. J.: Highly Acidic Ambient Particles, Soluble
511 Metals, and Oxidative Potential: A Link between Sulfate and Aerosol Toxicity, *Environ. Sci. Technol.*, 51,
512 2611-2620, 10.1021/acs.est.6b06151, 2017.
- 513 Fu, H. and Chen, J.: Formation, features and controlling strategies of severe haze-fog pollutions in China, *Sci.*
514 *Total Environ.*, 578, 121-138, <https://doi.org/10.1016/j.scitotenv.2016.10.201>, 2017.
- 515 Gao, J., Wei, Y., Shi, G., Yu, H., Zhang, Z., Song, S., Wang, W., Liang, D., and Feng, Y.: Roles of RH, aerosol pH
516 and sources in concentrations of secondary inorganic aerosols, during different pollution periods, *Atmos.*
517 *Environ.*, 241, 117770, <https://doi.org/10.1016/j.atmosenv.2020.117770>, 2020.
- 518 Ge, B., Xu, X., Ma, Z., Pan, X., Wang, Z., Lin, W., Ouyang, B., Xu, D., Lee, J., Zheng, M., Ji, D., Sun, Y., Dong,
519 H., Squires, F. A., Fu, P., and Wang, Z.: Role of Ammonia on the Feedback Between AWC and Inorganic
520 Aerosol Formation During Heavy Pollution in the North China Plain, *Earth Space Sci.*, 6, 1675-1693,
521 <https://doi.org/10.1029/2019EA000799>, 2019.
- 522 Guo, H., Liu, J., Froyd, K. D., Roberts, J. M., Veres, P. R., Hayes, P. L., Jimenez, J. L., Nenes, A., and Weber, R.
523 J.: Fine particle pH and gas-particle phase partitioning of inorganic species in Pasadena, California, during
524 the 2010 CalNex campaign, *Atmos. Chem. Phys.*, 17, 5703-5719, 10.5194/acp-17-5703-2017, 2017.
- 525 Guo, H., Sullivan, A. P., Campuzano-Jost, P., Schroder, J. C., Lopez-Hilfiker, F. D., Dibb, J. E., Jimenez, J. L.,
526 Thornton, J. A., Brown, S. S., Nenes, A., and Weber, R. J.: Fine particle pH and the partitioning of nitric

527 acid during winter in the northeastern United States, *J. Geophys. Res.: Atmos.*
528 , 121, 10,355-310,376, <https://doi.org/10.1002/2016JD025311>, 2016.

529 Guo, S., Hu, M., Zamora, M. L., Peng, J., Shang, D., Zheng, J., Du, Z., Wu, Z., Shao, M., Zeng, L., Molina, M.
530 J., and Zhang, R.: Elucidating severe urban haze formation in China, *Proc. Natl. Acad. Sci. USA*, 111,
531 17373-17378, 10.1073/pnas.1419604111, 2014.

532 Gwynn, R. C., Burnett, R. T., and Thurston, G. D.: A time-series analysis of acidic particulate matter and daily
533 mortality and morbidity in the Buffalo, New York, region, *Environ. Health Persp.*, 108, 125-133,
534 doi:10.1289/ehp.00108125, 2000.

535 He, P., Xie, Z., Chi, X., Yu, X., Fan, S., Kang, H., Liu, C., and Zhan, H.: Atmospheric $\Delta^{17}\text{O}(\text{NO}_3^-)$ reveals
536 nocturnal chemistry dominates nitrate production in Beijing haze, *Atmos. Chem. Phys.*, 18, 14465-14476,
537 10.5194/acp-18-14465-2018, 2018.

538 Hodas, N., Sullivan, A. P., Skog, K., Keutsch, F. N., Collett, J. L., Decesari, S., Facchini, M. C., Carlton, A. G.,
539 Laaksonen, A., and Turpin, B. J.: Aerosol Liquid Water Driven by Anthropogenic Nitrate: Implications for
540 Lifetimes of Water-Soluble Organic Gases and Potential for Secondary Organic Aerosol Formation, *Environ.*
541 *Sci. Technol.*, 48, 11127-11136, 10.1021/es5025096, 2014.

542 Huang, R.-J., Duan, J., Li, Y., Chen, Q., Chen, Y., Tang, M., Yang, L., Ni, H., Lin, C., Xu, W., Liu, Y., Chen, C.,
543 Yan, Z., Ovadnevaite, J., Ceburnis, D., Dusek, U., Cao, J., Hoffmann, T., and O'Dowd, C. D.: Effects of
544 NH_3 and alkaline metals on the formation of particulate sulfate and nitrate in wintertime Beijing, *Sci. Total*
545 *Environ.*, 717, 137190, <https://doi.org/10.1016/j.scitotenv.2020.137190>, 2020.

546 Huang, R.-J., Zhang, Y., Bozzetti, C., Ho, K.-F., Cao, J.-J., Han, Y., Daellenbach, K. R., Slowik, J. G., Platt, S. M.,
547 Canonaco, F., Zotter, P., Wolf, R., Pieber, S. M., Brun, E. A., Crippa, M., Ciarelli, G., Piazzalunga, A.,
548 Schwikowski, M., Abbaszade, G., Schnelle-Kreis, J., Zimmermann, R., An, Z., Szidat, S., Baltensperger, U.,
549 Haddad, I. E., and Prévôt, A. S. H.: High secondary aerosol contribution to particulate pollution during haze
550 events in China, *Nature*, 514, 218-222, 10.1038/nature13774, 2014.

551 Huang, X., Qiu, R., Chan, C. K., and Ravi Kant, P.: Evidence of high $\text{PM}_{2.5}$ strong acidity in ammonia-rich
552 atmosphere of Guangzhou, China: Transition in pathways of ambient ammonia to form aerosol ammonium
553 at $[\text{NH}_4^+]/[\text{SO}_4^{2-}]=1.5$, *Atmos. Res.*, 99, 488-495, <https://doi.org/10.1016/j.atmosres.2010.11.021>, 2011.

554 Huang, X., Zhang, J., Luo, B., Wang, L., Tang, G., Liu, Z., Song, H., Zhang, W., Yuan, L., and Wang, Y.: Water-
555 soluble ions in $\text{PM}_{2.5}$ during spring haze and dust periods in Chengdu, China: Variations, nitrate formation
556 and potential source areas, *Environ. Pollut.*, 243, 1740-1749, <https://doi.org/10.1016/j.envpol.2018.09.126>,
557 2018.

558 Huie, R. E. and Neta, P.: Kinetics of one-electron transfer reactions involving chlorine dioxide and nitrogen
559 dioxide, *J. Phys. Chem.*, 90, 1193-1198, 10.1021/j100278a046, 1986.

560 Jacob, D. J.: Heterogeneous chemistry and tropospheric ozone, *Atmos. Environ.*, 34, 2131-2159,
561 [https://doi.org/10.1016/S1352-2310\(99\)00462-8](https://doi.org/10.1016/S1352-2310(99)00462-8), 2000.

562 Jin, X., Wang, Y., Li, Z., Zhang, F., Xu, W., Sun, Y., Fan, X., Chen, G., Wu, H., Ren, J., Wang, Q., and Cribb, M.:
563 Significant contribution of organics to aerosol liquid water content in winter in Beijing, China, *Atmos. Chem.*
564 *Phys.*, 20, 901-914, <https://doi.org/10.5194/acp-20-901-2020>, 2020.

565 Kanchan, K., Gorai, A. K., and Goyal, P.: A review on air quality indexing system, *Asian J Atmos. Environ.*, 9,
566 101-113, 2015.

567 Lavigne, E., Yasseen, A. S., Stieb, D. M., Hystad, P., van Donkelaar, A., Martin, R. V., Brook, J. R., Crouse, D.
568 L., Burnett, R. T., Chen, H., Weichenthal, S., Johnson, M., Villeneuve, P. J., and Walker, M.: Ambient air
569 pollution and adverse birth outcomes: Differences by maternal comorbidities, *Environ. Res.*, 148, 457-466,
570 <https://doi.org/10.1016/j.envres.2016.04.026>, 2016.

571 Lee, Y. and Schwartz, S.: Kinetics of oxidation of aqueous sulfur (IV) by nitrogen dioxide, Elsevier, New York,
572 pp 453-466 pp.1982.

573 Li, H., Cheng, J., Zhang, Q., Zheng, B., Zhang, Y., Zheng, G., and He, K.: Rapid transition in winter aerosol
574 composition in Beijing from 2014 to 2017: response to clean air actions, *Atmos. Chem. Phys.*, 19, 11485-
575 11499, 10.5194/acp-19-11485-2019, 2019.

576 Liu, M., Song, Y., Zhou, T., Xu, Z., Yan, C., Zheng, M., Wu, Z., Hu, M., Wu, Y., and Zhu, T.: Fine particle pH
577 during severe haze episodes in northern China, *Geophys. Res. Lett.*, 44, 5213-5221,
578 <https://doi.org/10.1002/2017GL073210>, 2017a.

579 Liu, M., Huang, X., Song, Y., Tang, J., Cao, J., Zhang, X., Zhang, Q., Wang, S., Xu, T., Kang, L., Cai, X., Zhang,
580 H., Yang, F., Wang, H., Yu, J. Z., Lau, A. K. H., He, L., Huang, X., Duan, L., Ding, A., Xue, L., Gao, J., Liu,
581 B., and Zhu, T.: Ammonia emission control in China would mitigate haze pollution and nitrogen deposition,
582 but worsen acid rain, *Proc. Natl. Acad. Sci. USA*, 116, 7760-7765, 10.1073/pnas.1814880116, 2019.

583 Liu, P., Ye, C., Xue, C., Zhang, C., Mu, Y., and Sun, X.: Formation mechanisms of atmospheric nitrate and sulfate
584 during the winter haze pollution periods in Beijing: gas-phase, heterogeneous and aqueous-phase chemistry,
585 *Atmos. Chem. Phys.*, 20, 4153-4165, 10.5194/acp-20-4153-2020, 2020.

586 Liu, T., Chan, A. W. H., and Abbatt, J. P. D.: Multiphase Oxidation of Sulfur Dioxide in Aerosol Particles:
587 Implications for Sulfate Formation in Polluted Environments, *Environ. Sci. Technol.*, 55, 4227-4242,
588 10.1021/acs.est.0c06496, 2021.

589 Liu, Z., Xie, Y., Hu, B., Wen, T., Xin, J., Li, X., and Wang, Y.: Size-resolved aerosol water-soluble ions during the
590 summer and winter seasons in Beijing: Formation mechanisms of secondary inorganic aerosols,
591 *Chemosphere*, 183, 119-131, <https://doi.org/10.1016/j.chemosphere.2017.05.095>, 2017b.

592 McNeill, V. F.: Aqueous Organic Chemistry in the Atmosphere: Sources and Chemical Processing of Organic
593 Aerosols, *Environ. Sci. Technol.*, 49, 1237-1244, 10.1021/es5043707, 2015.

594 Nenes, A., Pandis, S. N., Weber, R. J., and Russell, A.: Aerosol pH and liquid water content determine when
595 particulate matter is sensitive to ammonia and nitrate availability, *Atmos. Chem. Phys.*, 20, 3249-3258,
596 10.5194/acp-20-3249-2020, 2020.

597 Nguyen, T., Petters, M., Suda, S., Guo, H., Weber, R., and Carlton, A.: Trends in particle-phase liquid water during
598 the Southern Oxidant and Aerosol Study, *Atmos. Chem. Phys.*, 14, 10911-10930, 2014.

599 Nie, W., Ding, A. J., Xie, Y. N., Xu, Z., Mao, H., Kerminen, V. M., Zheng, L. F., Qi, X. M., Huang, X., Yang, X.
600 Q., Sun, J. N., Herrmann, E., Petäjä, T., Kulmala, M., and Fu, C. B.: Influence of biomass burning plumes
601 on HONO chemistry in eastern China, *Atmos. Chem. Phys.*, 15, 1147-1159, 10.5194/acp-15-1147-2015,
602 2015.

603 Nozière, B., Dziedzic, P., and Córdoba, A.: Inorganic ammonium salts and carbonate salts are efficient catalysts
604 for aldol condensation in atmospheric aerosols, *Phys. Chem. Chem. Phys.*, 12, 3864-3872,
605 10.1039/B924443C, 2010.

606 Pathak, R. K., Wu, W. S., and Wang, T.: Summertime PM_{2.5} ionic species in four major cities of China: nitrate
607 formation in an ammonia-deficient atmosphere, *Atmos. Chem. Phys.*, 9, 1711-1722, 10.5194/acp-9-1711-
608 2009, 2009.

609 Rumsey, I. C., Cowen, K. A., Walker, J. T., Kelly, T. J., Hanft, E. A., Mishoe, K., Rogers, C., Proost, R., Beachley,
610 G. M., Lear, G., Frelink, T., and Otjes, R. P.: An assessment of the performance of the Monitor for AeRosols
611 and GAses in ambient air (MARGA): a semi-continuous method for soluble compounds, *Atmos. Chem.*
612 *Phys.*, 14, 5639-5658, 10.5194/acp-14-5639-2014, 2014.

613 Shang, D., Peng, J., Guo, S., Wu, Z., and Hu, M.: Secondary aerosol formation in winter haze over the Beijing-
614 Tianjin-Hebei Region, China, *Front Env. Sci. Eng.*, 15, 34, 10.1007/s11783-020-1326-x, 2020.

615 Shi, G., Xu, J., Shi, X., Liu, B., Bi, X., Xiao, Z., Chen, K., Wen, J., Dong, S., Tian, Y., Feng, Y., Yu, H., Song, S.,
616 Zhao, Q., Gao, J., and Russell, A. G.: Aerosol pH Dynamics During Haze Periods in an Urban Environment
617 in China: Use of Detailed, Hourly, Speciated Observations to Study the Role of Ammonia Availability and
618 Secondary Aerosol Formation and Urban Environment, *J. Geophys. Res.: Atmos.*
619 , 124, 9730-9742, <https://doi.org/10.1029/2018JD029976>, 2019.

620 Shiraiwa, M., Pfrang, C., Koop, T., and Pöschl, U.: Kinetic multi-layer model of gas-particle interactions in
621 aerosols and clouds (KM-GAP): linking condensation, evaporation and chemical reactions of organics,
622 oxidants and water, *Atmos. Chem. Phys.*, 12, 2777-2794, 10.5194/acp-12-2777-2012, 2012.

623 Solera García, M. A., Timmis, R. J., Van Dijk, N., Whyatt, J. D., Leith, I. D., Leeson, S. R., Braban, C. F., Sheppard,
624 L. J., Sutton, M. A., and Tang, Y. S.: Directional passive ambient air monitoring of ammonia for fugitive
625 source attribution; a field trial with wind tunnel characteristics, *Atmos. Environ.*, 167, 576-585,
626 <https://doi.org/10.1016/j.atmosenv.2017.07.043>, 2017.

627 Song, C. H., Kim, C. M., Lee, Y. J., Carmichael, G. R., Lee, B. K., and Lee, D. S.: An evaluation of reaction
628 probabilities of sulfate and nitrate precursors onto East Asian dust particles, *J. Geophys. Res. Atmos.*, 112,
629 D18206, <https://doi.org/10.1029/2006JD008092>, 2007.

630 Song, S., Gao, M., Xu, W., Shao, J., Shi, G., Wang, S., Wang, Y., Sun, Y., and McElroy, M. B.: Fine-particle pH
631 for Beijing winter haze as inferred from different thermodynamic equilibrium models, *Atmos. Chem. Phys.*,
632 18, 7423-7438, 10.5194/acp-18-7423-2018, 2018.

633 Tan, H., Cai, M., Fan, Q., Liu, L., Li, F., Chan, P., Deng, X., and Wu, D.: An analysis of aerosol liquid water
634 content and related impact factors in Pearl River Delta, *Sci. Total Environ.*, 579, 1822-1830, 2017.

635 Wang, G., Zhang, R., Gomez, M. E., Yang, L., Zamora, M. L., Hu, M., Lin, Y., Peng, J., Guo, S., and Meng, J.:
636 Persistent sulfate formation from London Fog to Chinese haze, *Proc. Natl. Acad. Sci. USA*, 113, 13630-
637 13635, 2016.

638 Wang, G., Chen, J., Xu, J., Yun, L., Zhang, M., Li, H., Qin, X., Deng, C., Zheng, H., Gui, H., Liu, J., and Huang,
639 K.: Atmospheric Processing at the Sea-Land Interface Over the South China Sea: Secondary Aerosol
640 Formation, Aerosol Acidity, and Role of Sea Salts, *J. Geophys. Res.: Atmos.*
641 , 127, e2021JD036255, <https://doi.org/10.1029/2021JD036255>, 2022.

642 Wang, H., Wang, X., Zhou, H., Ma, H., Xie, F., Zhou, X., Fan, Q., Lü, C., and He, J.: Stoichiometric characteristics
643 and economic implications of water-soluble ions in PM_{2.5} from a resource-dependent city, *Environ. Res.*,
644 193, 110522, <https://doi.org/10.1016/j.envres.2020.110522>, 2021.

645 Wang, J., Li, J., Ye, J., Zhao, J., and Jacob, D. J.: Fast sulfate formation from oxidation of SO₂ by NO₂ and HONO
646 observed in Beijing haze, *Nat. Commun.*, 11, 2844, 2020.

647 Wang, S., Nan, J., Shi, C., Fu, Q., Gao, S., Wang, D., Cui, H., Saiz-Lopez, A., and Zhou, B.: Atmospheric ammonia
648 and its impacts on regional air quality over the megacity of Shanghai, China, *Sci. Rep.*, 5, 15842,
649 10.1038/srep15842, 2015.

650 Weber, R. J., Guo, H., Russell, A. G., and Nenes, A.: High aerosol acidity despite declining atmospheric sulfate
651 concentrations over the past 15 years, *Nat. Geosci.*, 9, 282-285, 10.1038/ngeo2665, 2016.

652 Wong, J. P. S., Lee, A. K. Y., and Abbatt, J. P. D.: Impacts of Sulfate Seed Acidity and Water Content on Isoprene
653 Secondary Organic Aerosol Formation, *Environ. Sci. Technol.*, 49, 13215-13221, 10.1021/acs.est.5b02686,
654 2015.

655 Wu, Z., Wang, Y., Tan, T., Zhu, Y., Li, M., Shang, D., Wang, H., Lu, K., Guo, S., Zeng, L., and Zhang, Y.: Aerosol
656 Liquid Water Driven by Anthropogenic Inorganic Salts: Implying Its Key Role in Haze Formation over the
657 North China Plain, *Environ. Sci. Technol. Lett.*, 5, 160-166, 10.1021/acs.estlett.8b00021, 2018.

658 Xie, F., Zhou, X., Wang, H., Gao, J., Hao, F., He, J., and Lü, C.: Heating events drive the seasonal patterns of

659 volatile organic compounds in a typical semi-arid city, *Sci. Total Environ.*, 788, 147781,
660 <https://doi.org/10.1016/j.scitotenv.2021.147781>, 2021.

661 Xie, Y., Wang, G., Wang, X., Chen, J., Chen, Y., Tang, G., Wang, L., Ge, S., Xue, G., Wang, Y., and Gao, J.:
662 Nitrate-dominated PM_{2.5} and elevation of particle pH observed in urban Beijing during the winter of 2017,
663 *Atmos. Chem. Phys.*, 20, 5019-5033, 10.5194/acp-20-5019-2020, 2020.

664 Xu, L., Duan, F., He, K., Ma, Y., Zhu, L., Zheng, Y., Huang, T., Kimoto, T., Ma, T., Li, H., Ye, S., Yang, S., Sun,
665 Z., and Xu, B.: Characteristics of the secondary water-soluble ions in a typical autumn haze in Beijing,
666 *Environ. Pollut.*, 227, 296-305, <https://doi.org/10.1016/j.envpol.2017.04.076>, 2017.

667 Xue, J., Griffith, S. M., Yu, X., Lau, A. K. H., and Yu, J. Z.: Effect of nitrate and sulfate relative abundance in
668 PM_{2.5} on liquid water content explored through half-hourly observations of inorganic soluble aerosols at a
669 polluted receptor site, *Atmos. Environ.*, 99, 24-31, <https://doi.org/10.1016/j.atmosenv.2014.09.049>, 2014.

670 Xue, J., Yuan, Z., Griffith, S. M., Yu, X., Lau, A. K. H., and Yu, J. Z.: Sulfate Formation Enhanced by a Cocktail
671 of High NO_x, SO₂, Particulate Matter, and Droplet pH during Haze-Fog Events in Megacities in China: An
672 Observation-Based Modeling Investigation, *Environ. Sci. Technol.*, 50, 7325-7334,
673 10.1021/acs.est.6b00768, 2016.

674 Yao, L., Fan, X., Yan, C., Kurtén, T., Daellenbach, K. R., Li, C., Wang, Y., Guo, Y., Dada, L., Rissanen, M. P., Cai,
675 J., Tham, Y. J., Zha, Q., Zhang, S., Du, W., Yu, M., Zheng, F., Zhou, Y., Kontkanen, J., Chan, T., Shen, J.,
676 Kujansuu, J. T., Kangasluoma, J., Jiang, J., Wang, L., Worsnop, D. R., Petäjä, T., Kerminen, V.-M., Liu, Y.,
677 Chu, B., He, H., Kulmala, M., and Bianchi, F.: Unprecedented Ambient Sulfur Trioxide (SO₃) Detection:
678 Possible Formation Mechanism and Atmospheric Implications, *Environ. Sci. Technol. Lett.*, 7, 809-818,
679 10.1021/acs.estlett.0c00615, 2020.

680 Yue, F., He, P., Chi, X., Wang, L., Yu, X., Zhang, P., and Xie, Z.: Characteristics and major influencing factors of
681 sulfate production via heterogeneous transition-metal-catalyzed oxidation during haze evolution in China,
682 *Atmos. Pollut. Res.*, 11, 1351-1358, <https://doi.org/10.1016/j.apr.2020.05.014>, 2020.

683 Zhai, S., Jacob, D. J., Wang, X., Liu, Z., Wen, T., Shah, V., Li, K., Moch, J. M., Bates, K. H., Song, S., Shen, L.,
684 Zhang, Y., Luo, G., Yu, F., Sun, Y., Wang, L., Qi, M., Tao, J., Gui, K., Xu, H., Zhang, Q., Zhao, T., Wang,
685 Y., Lee, H. C., Choi, H., and Liao, H.: Control of particulate nitrate air pollution in China, *Nat. Geosci.*,
686 10.1038/s41561-021-00726-z, 2021.

687 Zhang, R., Wang, G., Guo, S., Zamora, M. L., Ying, Q., Lin, Y., Wang, W., Hu, M., and Wang, Y.: Formation of
688 Urban Fine Particulate Matter, *Chem. Rev.*, 115, 3803-3855, 10.1021/acs.chemrev.5b00067, 2015.

689 Zhao, Q., Nenes, A., Yu, H., Song, S., Xiao, Z., Chen, K., Shi, G., Feng, Y., and Russell, A. G.: Using High-
690 Temporal-Resolution Ambient Data to Investigate Gas-Particle Partitioning of Ammonium over Different
691 Seasons, *Environ. Sci. Technol.*, 54, 9834-9843, 10.1021/acs.est.9b07302, 2020.

692 Zheng, B., Zhang, Q., Zhang, Y., He, K., Wang, K., Zheng, G., Duan, F., Ma, Y., and Kimoto, T.: Heterogeneous
693 chemistry: a mechanism missing in current models to explain secondary inorganic aerosol formation during
694 the January 2013 haze episode in North China, *Atmos. Chem. Phys.*, 15, 2031-2049, 2015a.

695 Zheng, G. J., Duan, F. K., Su, H., Ma, Y. L., Cheng, Y., Zheng, B., Zhang, Q., Huang, T., Kimoto, T., Chang, D.,
696 Pöschl, U., Cheng, Y. F., and He, K. B.: Exploring the severe winter haze in Beijing: the impact of synoptic
697 weather, regional transport and heterogeneous reactions, *Atmos. Chem. Phys.*, 15, 2969-2983, 2015b.

698 Zhou, H., Lü, C., He, J., Gao, M., Zhao, B., Ren, L., Zhang, L., Fan, Q., Liu, T., He, Z., Dudagula, Zhou, B., Liu,
699 H., and Zhang, Y.: Stoichiometry of water-soluble ions in PM_{2.5}: Application in source apportionment for a
700 typical industrial city in semi-arid region, Northwest China, *Atmos. Res.*, 204, 149-160,
701 <https://doi.org/10.1016/j.atmosres.2018.01.017>, 2018.

702 Zhu, Y., Li, W., Lin, Q., Yuan, Q., Liu, L., Zhang, J., Zhang, Y., Shao, L., Niu, H., Yang, S., and Shi, Z.: Iron

703 solubility in fine particles associated with secondary acidic aerosols in east China, Environ. Pollut., 264,
704 114769, <https://doi.org/10.1016/j.envpol.2020.114769>, 2020.
705